machines

MDPI

Article

ANN-Based Performance Modeling of a Solar Air Collector with Varying Absorber Surfaces

Filiz Ozgen [1], Zeynep Bala Duranay [2,*], Ayse Dayan [1] and Hanifi Güldemir [2]

[1] Department of Mechanical Engineering, Technology Faculty, Firat University, Elazig 23119, Türkiye; fozgen@firat.edu.tr (F.O.); aysedayan.96@gmail.com (A.D.)
[2] Electrical Electronics Engineering Department, Technology Faculty, Firat University, Elazig 23119, Türkiye; hguldemir@firat.edu.tr
* Correspondence: zbduranay@firat.edu.tr

Abstract

In this study, an Artificial Neural Network (ANN) approach was employed to predict the outlet air temperature and thermal efficiency of a solar air collector equipped with porous absorber surfaces. The experimental data used for model development were obtained from a custom-built solar air collector whose absorber surface was constructed using porous metallic scourers. Three different absorber surface configurations were tested under varying operating conditions. The dataset included measurements of inlet air temperature, solar irradiance, air mass flow rate, and surface temperatures recorded at four distinct points on the absorber. Corresponding outlet air temperatures and thermal efficiency values were also determined experimentally. ANN models were trained using this dataset, and the prediction results were graphically compared with experimental outcomes for all three surface types. To further evaluate the model's performance, test data were utilized, and the results were assessed using the correlation coefficient (R) and mean squared error (MSE) metrics. The ANN model demonstrated high predictive accuracy, yielding an R value of 0.99987 and an MSE of 0.0901.

Keywords: absorber surface; artificial neural networks; porous absorber surfaces; solar collector

check for updates

Academic Editors: Ignacio Martin-Diaz and Kim Tiow Ooi

Received: 29 July 2025
Revised: 24 August 2025
Accepted: 2 September 2025
Published: 4 September 2025

Citation: Ozgen, F.; Duranay, Z.B.; Dayan, A.; Güldemir, H. ANN-Based Performance Modeling of a Solar Air Collector with Varying Absorber Surfaces. *Machines* **2025**, *13*, 812. https://doi.org/10.3390/machines13090812

Copyright: © 2025 by the authors. Licensee MDPI, Basel, Switzerland. This article is an open access article distributed under the terms and conditions of the Creative Commons Attribution (CC BY) license (https://creativecommons.org/licenses/by/4.0/).

1. Introduction

Solar energy, being a clean and sustainable resource, has significantly lower environmental impact compared to conventional energy sources. Its utilization spans a wide range of thermal applications, including water and air heating, drying, distillation, agricultural greenhouse heating, cooking, water pumping, space heating and cooling, salt production, photochemical and photobiological processes, and even hydrogen generation. At higher temperatures, solar-heated fluids can also be employed for electricity generation and industrial heating processes.

Among the technologies that convert solar radiation into usable thermal energy, solar air heaters, also referred to as solar air collectors (SACs), stand out as practical and widely used systems, particularly for low-temperature applications [1]. These systems function as heat exchangers, where the primary components include a transparent cover and a black absorber surface that captures solar radiation and transfers heat to the air passing through the system. One major advantage of SACs is that the working fluid air, does not freeze or boil, making them reliable in various climates [2].

However, the relatively low thermal conductivity and specific heat of air limit the convective heat transfer from the absorber surface, leading to generally low thermal efficiency. To address this limitation, researchers have explored numerous strategies to enhance thermal performance [3–7]. These efforts include modifying the absorber surface geometry through the use of corrugated surfaces, obstacles, baffles, V-grooves, ribs, finned structures, and surface treatments. Such modifications help to increase turbulence, improve heat transfer rates, and ensure better distribution of airflow within the collector.

In addition to surface modifications, variations in material, shape, size, and overall design of the collectors have also been tested. For example, double-flow SAC designs have been introduced to increase the heat transfer area, further boosting thermal efficiency [8,9]. A study presented in [10] developed models for the Nusselt number and friction factor in solar air collectors with inclined baffles, demonstrating the effectiveness of specific geometrical enhancements.

While various optimization techniques exist, intelligent system design using artificial neural networks (ANN) methods offers a rapid and accurate solution for modeling, simulation, and control of complex, nonlinear systems. The review underscored the suitability and effectiveness of ANN methodologies for solar collector performance prediction and suggested directions for future research.

Esen et al. [11] applied ANN to model a solar air collector and validated their results against experimental data. Utilizing various ANN architectures, they optimized model parameters and established validation criteria. Comparing the model's predictions with experimental data showed that the ANN could effectively estimate key aspects of SAC system performance with reasonable accuracy.

Diez et al. [12] applied ANN techniques to model a flat surface solar collector for different fluid flow rates. The model utilized inputs such as solar irradiance, ambient temperature, inlet fluid temperature, and fluid flow rate to predict outlet temperature. The results confirmed that the ANN approach yielded high-accuracy predictions across multiple flow conditions.

Delfani et al. [13] implemented an ANN-based method to forecast the performance of a nanofluid-based direct absorption solar collector. Experimental testing involved nine collector prototypes with varying depths and lengths, generating a comprehensive dataset for network training. Inputs comprised collector depth, length, fluid flow rate, nanoparticle concentration, and reduced temperature difference, while outputs included collector efficiency and Nusselt number. Findings revealed that increased collector depth enhanced efficiency by approximately 9%, while collector length had negligible impact. The ANN model showed strong agreement with experimental data, affirming its efficacy in performance prediction for direct absorption collectors.

Wang et al. [14] optimized the thermal performance of parabolic trough solar collector systems using a hybrid genetic algorithm–backpropagation neural network model. The evaluation metrics included system output energy, thermal efficiency, and heat loss, leading to the development of a reliable prediction model. Optimization results indicated that the optimized geometrical configuration significantly improved the system's thermal efficiency.

In [15], Ghritlahre et al. provided a comprehensive overview of ANN-based methods used for the performance prediction of solar collector systems. As solar collectors constitute fundamental components in low-temperature to medium-temperature solar energy systems, optimal design is critical for achieving efficient performance.

Castilla et al. [16] proposed a digital twin system for flat surface solar collectors based on ANN modeling. The system aims to reduce carbon dioxide emissions in bioclimatic buildings and facilitate their transition to Zero Energy Buildings. The ANN-based prediction model was calibrated and validated using one year of operational data covering

diverse weather conditions including sunny, cloudy, partly cloudy, and non-operational days. Validation employing multiple statistical metrics confirmed the model's robustness and its applicability for system operation and control.

Sun et al. [17] conducted a numerical analysis of the exergy performance of a hybrid solar energy system equipped with surface and sinusoidal tube collectors, utilizing ANN techniques. Integration of photovoltaic–thermal (PVT) collectors with cooling systems offers simultaneous generation of electrical and thermal energy, potentially reducing exergy consumption in the building sector. The concurrent application of nanofluid usage and geometric modifications produced synergistic improvements in PVT performance, contributing to reductions in system size and cost. The study employed ANN models to accurately predict PVT system performance across specified Reynolds numbers and nanofluid concentrations.

Du et al. [18] presented an analysis of solar collector performance using ANN models combined with data clustering techniques. Accurate prediction of solar collector efficiency is vital for optimal design and operation of solar heating systems. Utilizing a next-generation glass tube solar collector as a reference, experimental measurements of performance across different weather scenarios were obtained and subjected to clustering analysis to eliminate outliers. The cleaned dataset was employed for training and validation of the ANN models, with input parameters including solar irradiance, ambient temperature, wind speed, fluid flow rate, and inlet fluid temperature. Results demonstrated that the integration of data clustering significantly enhanced prediction accuracy, providing a robust performance estimation method for solar collectors.

Naveenkumar et al. [19] provided a comprehensive review of recent advancements in solar water heaters and solar collectors, focusing on experimental and ANN-based modeling approaches. Given their numerous advantages over conventional energy sources, these renewable technologies have garnered significant research interest. Various system enhancements have been pursued to enhance thermal performance and efficiency. Research findings highlighted the role of ANN-based methods in supporting technological innovations and enhancing the performance and economic feasibility of solar thermal systems, thereby promoting wider adoption as sustainable energy solutions.

In light of the reviewed literature, it is evident that ANN-based modeling has become a powerful tool for predicting the thermal performance of various solar collector configurations. Numerous studies have demonstrated the effectiveness of ANN models in handling nonlinear relationships between input parameters and system performance metrics. However, relatively limited attention has been given to air-based solar collectors incorporating porous absorber surfaces formed from metallic scourers, despite their potential to enhance heat transfer through increased surface area and turbulence.

In this context, the present study aims to develop and validate an ANN model to accurately predict the outlet air temperature and thermal efficiency of a solar air collector equipped with three distinct porous absorber surface configurations. Experimental data obtained from a custom-designed SAC prototype constructed using steel scourers as porous media were used to train, validate, and test the model. The inputs included operating variables such as mass flow rate, inlet temperature, absorber surface temperatures, and solar irradiance, while the outputs were outlet air temperature and thermal efficiency.

The novelty of this work lies in its focus on modeling a SAC system with non-traditional porous absorber geometry and providing a detailed performance evaluation based on commonly used performance metrics. The proposed ANN model demonstrates strong predictive capability and generalization across varying operating conditions.

This study not only confirms the suitability of ANN for such complex thermal systems but also offers a practical, low-cost pathway for performance forecasting in SAC designs

employing unconventional absorber structures. The findings contribute to the growing body of literature on intelligent system modeling for solar technologies and may assist in improving and refining the performance of advanced solar thermal systems.

2. Experimental Study

This research employed experimental data from [20] to predict the outlet air temperature and thermal efficiency of a solar air collector with porous absorber surfaces using an ANN. The referenced experimental work involved measurements from three different absorber surface configurations under varying operating conditions. The thermal performance of an air-based solar collector with a porous scourers absorber surface was investigated. The collector's casing measures 120 cm in length, 80 cm in width, and 40 cm in height. A 4 mm thick window glass was used as the transparent cover, while the casing was constructed from plywood. For insulation, 3 cm thick Styrofoam was employed. Chipboard, as a composite material, provides advantages in terms of machinability and formability due to its homogeneous structure. In addition to being lightweight and low-cost, it offers a certain degree of sound and thermal insulation. Styrofoam, being a lightweight and porous thermal insulation material, is widely used to reduce heat losses due to its high thermal resistance and low thermal conductivity. It is also resistant to impacts; therefore, it was chosen as the insulation material for the collector casing. The outer side edges and bottom of the collector casing were made of aluminum, and these surfaces exposed to the external environment were tightly insulated with the insulation material. The collector was oriented southward with an inclination angle of 38° relative to the horizontal plane. In the study, three different absorber surfaces were utilized. The surfaces were fabricated to allow airflow on both sides of the absorber. The air passage channels of the solar air collector, and consequently the absorber sur-face, were formed using porous metallic scourers. These metallic scourers were glued side by side and end to end in a solenoid form and subsequently coated with matte black paint. The rationale behind selecting such absorber surfaces is based on literature findings indicating that air flow through dual channels enhances collector efficiency. The experimental setup used in [20] is presented in Figure 1.

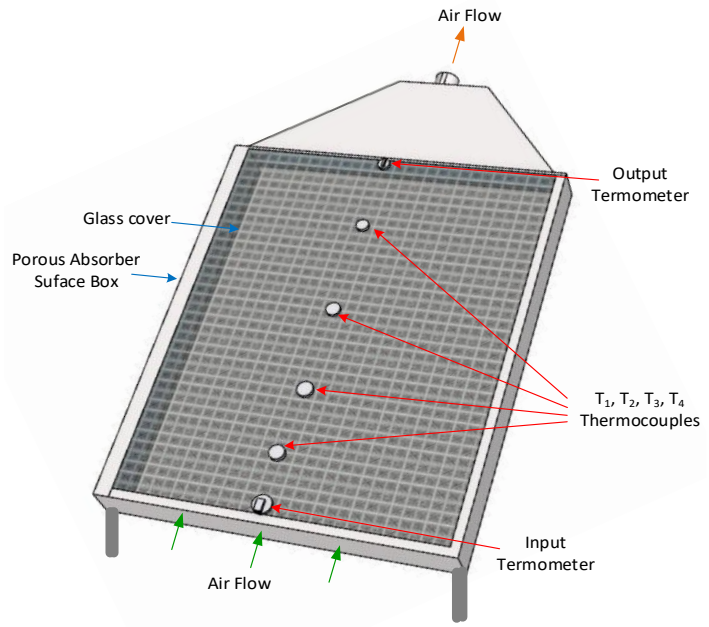


Figure 1. Schematic of experimental setup.

In the experimental study performed in [20], to construct the absorber surfaces, 180 porous metallic scourers were collected and adhered to both the top and bottom sides

of a 1.5 mm thick galvanized sheet metal using a type of silicone adhesive. Following the adhesion process, the sheet metal was coated with matte black paint to form the absorber surface. The first absorber surface (Type I) included a total of 102 scourers arranged in a complex pattern, as shown in Figure 2a. The second absorber surface (Type II) consisted of 78 scourers arranged in an orderly row, depicted in Figure 2b, while the third absorber surface (Type III), shown in Figure 2c, was a flat surface without any scourers attached.



(**a**) (**b**) (**c**)

Figure 2. Absorber surfaces used in experiments: (**a**) Type I, (**b**) Type II, (**c**) Type III [20].

The test rig for experimental study, described in [20], includes a CM3 pyranometer manufactured by Kipp & Zonen, Sterling-USA, to obtain the total solar irradiance incident on a unit horizontal surface. The collector was connected via a duct to the inlet of an air circulation fan with a flow rate of 800 m^3/h. A digital anemometer, AM-4206M produced by Lutron EA Ltd. in London, England, equipped with a metal-bladed fan at its head was installed at the fan inlet to measure airflow rate and velocity. This device operates on the hot-wire principle and can measure even low-speed airflows with high precision. With an accuracy of $\pm$(0.5% + 0.1 m/s), it can measure within a range of 0.1–25 m/s. In addition to its digital display enabling real-time readings, its portable design makes it widely preferred in laboratory and field applications. The air temperatures at the inlet and outlet of the collector were measured using mercury thermometers with a range of 0–100 °C. Temperature measurements were made at specific points on the absorber surfaces. Four T-type Cu-Constantan thermocouples were attached at equal intervals of 24 cm, and the other ends were connected to a CR510 data logger produced by Campbell Scientific in North Logan, USA, for recording temperature values. These thermocouples, offering high precision and stability within the measurement range of −200 °C to 350 °C, are commonly used in energy systems. Chosen for their low cost and reliability, Type T thermocouples were positioned at different points on the absorber plate to determine temperature distributions. The data logger is equipped with a high voltage source (up to 7751 V) and a low current source (0–50 mA), with a temperature measurement range between −200 °C and 630 °C. All thermocouples were connected to the data logger, and the measurements were recorded with the aid of a computer. A water U-manometer was employed to determine the pressure losses between the inlet and outlet sides of the collector. Additionally, a rotameter was installed at the outlet of the fan that draws air through the collector to measure the air flow rate, and a dimmer was used to adjust the flow rate. During the experiments, the dimmer controlled the fan supply voltage, thereby regulating the airflow.

The experiments were conducted in August between 9:00 a.m. and 4:00 p.m. at half-hour intervals. During the experiments, the inlet and outlet temperatures of the collector, the temperature values at four different points on the absorber surface, and the radiation values were measured and transferred to the computer with the aid of a data logger. The

experiments were carried out continuously, and each continuous measurement test lasted for 7 h, as also described in [20].

As a result of the experimental studies, in total, 30 data samples (15 for each mass flow rate of 0.05 and 0.025 kg/s) were collected per surface type, yielding 90 samples overall.

3. ANN Based Analysis of Solar Air Collector

ANNs are powerful and robust computational systems inspired by the structure and functioning of biological neural networks in the human brain. These networks find extensive applications in engineering, education, science, and data-driven analysis due to their capability to identify and represent intricate nonlinear interactions between inputs and outputs [21–25]. An ANN consists of multiple layers of linked processing elements known as neurons or nodes. The units are arranged into three primary layer types: the input layer, one or several hidden layers, and the output layer.

The input layer receives the external signals—also called input features or parameters—which are then transmitted to the subsequent layers. Each neuron in the hidden layers processes inputs using a weighted sum followed by an activation function (e.g., sigmoid, ReLU, or tanh), enabling the network to model nonlinear dependencies within the data. The hidden layers are where learning and abstraction occur, allowing the network to discover patterns, interactions, and high-level representations that may not be apparent through traditional methods.

The output layer generates the ultimate prediction or categorization by utilizing the patterns learned during training. The quantity of neurons in this layer varies according to the problem type, for instance, a single neuron for regression problems or several neurons for classification tasks. During training, the ANN learns by adjusting the weights of connections between neurons using a learning algorithm, most commonly backpropagation combined with optimization methods such as the Levenberg–Marquardt or gradient descent.

A significant feature of ANNs lies in their generalization ability, that is, their capacity to make accurate predictions on unseen data after being trained on a limited dataset. This makes them highly suitable for modeling systems with nonlinear, multi-variable, or experimentally expensive behaviors, such as thermal processes, material behavior, or energy systems.

In this research, an ANN framework was created to forecast the thermal efficiency of a solar air collector equipped with porous scourers absorber surfaces. The network was designed using MATLAB R2023 Version's Neural Network Toolbox (nnstart), where a feedforward backpropagation architecture was applied. The model includes eight input parameters and two output parameters as shown in Figure 3. Input parameters consist of the surface type (categorical), mass flow rate, m (kg/s), inlet air temperature, T_{in} (°C), four separate temperature measurements from different points on the absorber surface (T_1, T_2, T_3, T_4 (°C)), and solar irradiance, Irr (W/m^2). These parameters represent the operational and geometric conditions of the collector. The output parameters are the outlet air temperature, T_{out} (°C) and the thermal efficiency, η (%), which characterize the system's overall performance. In Figure 3, in the ANN model, b and w represent biases and weights of the ANN.

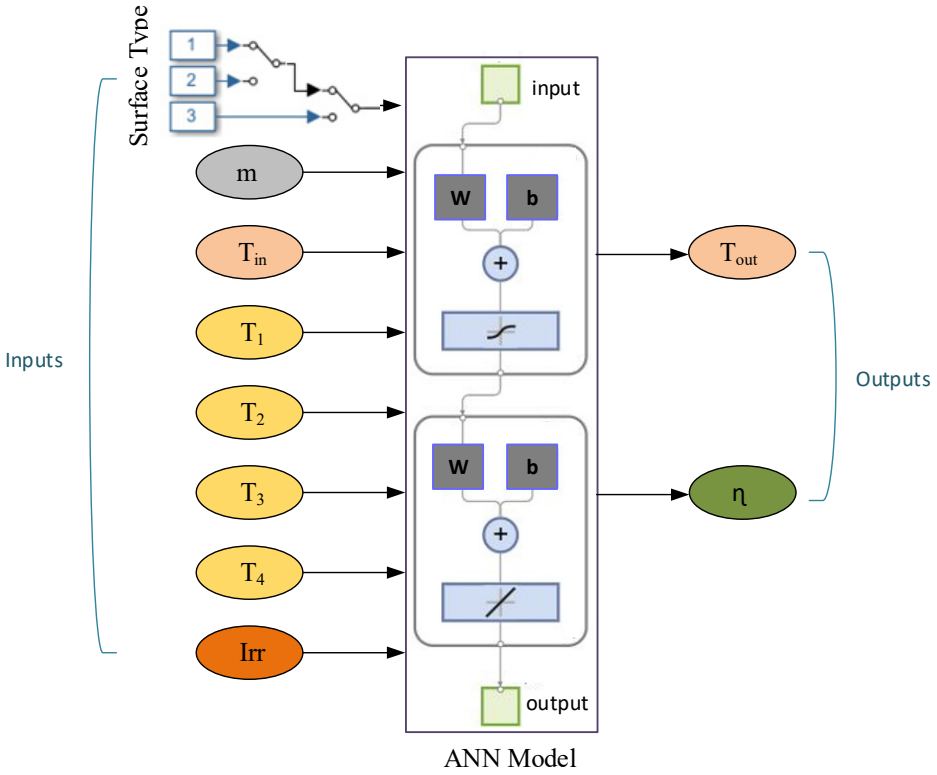


Figure 3. ANN based prediction model.

The ANN developed in this study consisted of a single hidden layer with 5 neurons, employing the sigmoid activation function to capture nonlinear dependencies. The output layer used a linear activation function, which is appropriate for continuous-valued regression outputs such as T_{out} and η . A total of 90 experimental data points were used to train, validate, and test the model. The dataset was randomly divided into 80% training (72 samples), 10% validation (9 samples), and 10% testing (9 samples). Training was performed using the Levenberg–Marquardt backpropagation algorithm with a maximum of 1000 epochs. The best validation performance was achieved at epoch 5, and the training was stopped at epoch 11 according to the validation stopping criterion. The corresponding training performance curve is presented in Figure 4, where the mean squared error (MSE) evolution for training, validation, and test subsets can be observed.

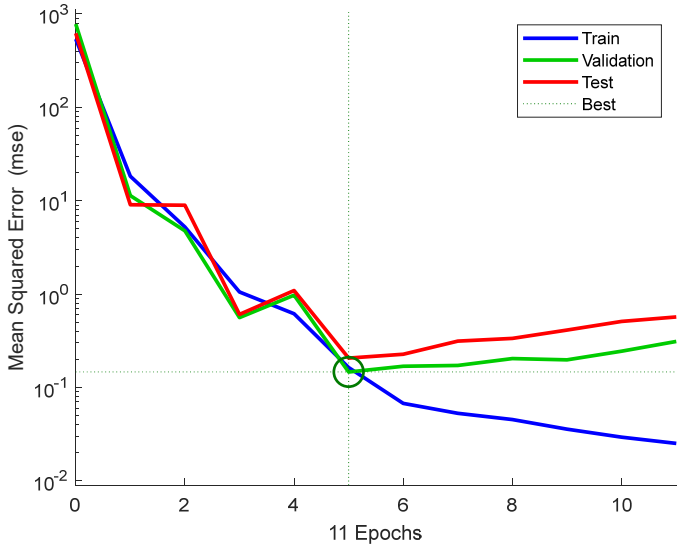


Figure 4. Performance curve of the ANN model.

The circled point in Figure 4 marks the best validation epoch (5), and the early-stopping mechanism terminated the training at epoch 11. The training and validation errors decreased concurrently and did not diverge, while the test error followed the same trend, confirming that the model generalized well and did not suffer from overfitting despite the limited dataset size. The total number of trainable parameters (weights and biases) was 57, which were optimized during training.

Although the dataset size may appear limited, the relatively simple ANN architecture (single hidden layer with 5 neurons) requires fewer samples for stable convergence. Furthermore, the obtained accuracy metrics demonstrate that the model generalizes well, confirming that the chosen dataset size was sufficient for training and validation. A single hidden layer was intentionally selected, as it provides sufficient capacity to capture nonlinear dependencies while avoiding overfitting, which could arise with deeper architectures given the limited dataset. Similar dataset sizes have also been successfully used in ANN-based modeling of thermal and energy systems in the literature [9,11,22].

The chosen input features were selected based on their strong influence on the thermodynamic behavior of the system. By integrating both environmental variables (e.g., solar irradiance, inlet temperature) and physical characteristics (e.g., surface type, internal absorber temperatures), the ANN model is capable of capturing nonlinear interactions that are otherwise difficult to express through classical mathematical models. This flexible and adaptive nature of ANN makes it particularly valuable for systems like SACs, where multiple variables simultaneously affect performance.

To evaluate the precision of the ANN system, several evaluation metrics were employed. The model's predictive performance was quantitatively assessed using two key statistical metrics: MSE, and R [21]. MSE indicates the mean of the squared differences between the predicted and observed values. It assigns greater weight to larger errors, making it a sensitive measure of inaccurate predictions. MSE is defined as

$$MSE = \frac{1}{n}\sum_{i=1}^{n}(y_i - y_i')^2 \tag{1}$$

where y_i and y_i' denote the observed and predicted values, respectively, and n is the total number of samples. A smaller MSE indicates that the predicted values are closer to the actual data.

The correlation coefficient (R) quantifies the strength and direction of the linear relationship between the ANN outputs and the actual observed data. R is given by

$$R = \frac{\sum_{i=1}^{n}(y_i - \overline{y_i})(y_i' - \overline{y_i'})}{\sqrt{\sum_{i=1}^{n}(y_i - \overline{y_i})^2 \sum_{i=1}^{n}(y_i' - \overline{y_i'})^2}} \tag{2}$$

where $\overline{y_i}$ and $\overline{y_i'}$ are the mean values of the observed and predicted data, respectively. R values close to +1 indicate strong positive correlation between predictions and experimental data. For completeness, the coefficient of determination (R^2) can be directly obtained by squaring R in simple regression.

4. Simulation Results of ANN Predictions

The ANN model was trained using 90 experimental data points obtained from a solar air collector system with porous absorber surfaces formed using steel scourers. Three types of surfaces were tested: complex (Type I), moderately complex (Type II), and plain (Type III), with different arrangements of metallic scourers. The experimental setup was subjected to two different mass flow rates: 0.025 kg/s and 0.05 kg/s. Temperatures from

four different locations on the absorber surface were recorded, along with the inlet air temperature and solar irradiance. These measurements formed the basis for the input layer of the ANN.

The application of ANN in this research aimed to establish a fast and reliable predictive model for estimating the outlet air temperature and thermal efficiency of the solar air collector system under varying conditions. Traditional modeling approaches often struggle with the nonlinear and multivariable nature of solar thermal systems. In contrast, ANN can effectively handle these complexities and provide accurate predictions once trained on experimental data. This makes ANN an excellent alternative to time-consuming and costly repeated experiments, especially when design optimization or real-time predictions are required [21,22].

Once the model was trained and tested, it was used to predict the outlet air temperature and thermal efficiency under varying operational conditions. The simulation outputs were compared with actual experimental values to evaluate model performance. The ANN demonstrated excellent predictive capabilities across all data partitions.

Figure 5 presents the correlation plots corresponding to the training, validation, testing, and overall stages of the ANN model. As seen in the figure, there is a strong correlation between the predicted and experimental values, with R approaching 0.99993 across all phases. The dashed line (Y = T) in each subplot denotes the perfect fit reference, where predicted values are equal to the targets. The consistently high R values—around 0.99—indicate that the model performs with a high degree of accuracy and generalizes well to unseen data, showing no signs of overfitting or underfitting.

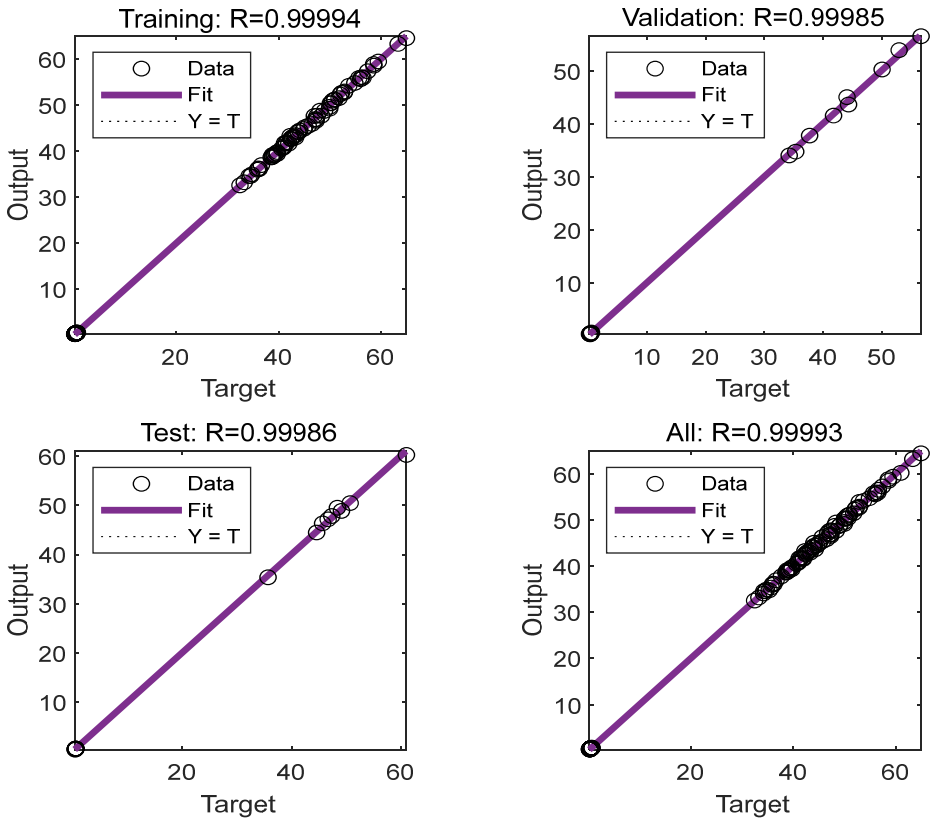


Figure 5. Correlation plots of the ANN model for training, validation, test and all datasets.

In addition to high R values, the MSE was consistently low, typically remaining below 0.0863 for both output parameters. MSE quantifies the average size of the prediction errors in the same units as the target variables, offering intuitive insight into model precision.

Smaller MSE values signify that the predicted results closely match the observed data, even under different operating conditions.

Together, the high R values and low MSE confirm the robustness, precision, and generalization ability of the ANN architecture. These findings support the use of ANNs as an effective modeling tool for simulating the complex thermal behavior of SACs with porous scourers absorbers.

Figure 6 illustrates the error histogram of the ANN model, depicting the distribution of prediction errors across the training, validation, and testing datasets. The histogram is divided into 20 bins, which represent intervals grouping the prediction errors into specific ranges. This binning allows for a clearer visualization of how frequently different error magnitudes occur.

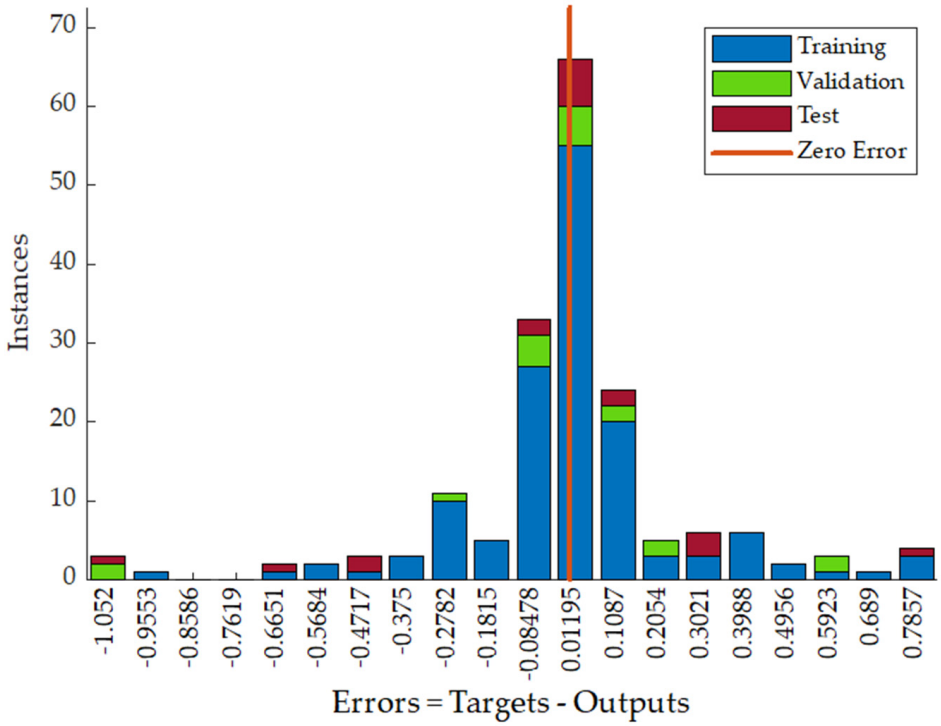
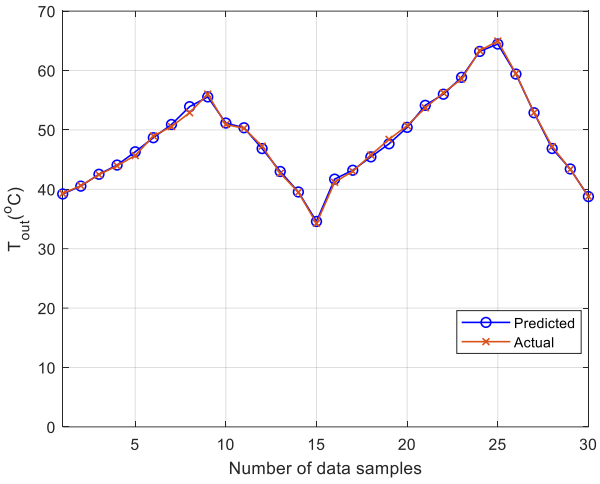


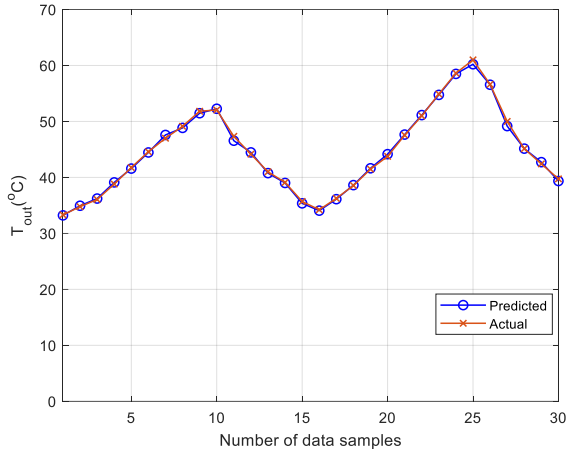
Figure 6. Error histogram showing the distribution of prediction errors of the ANN model.

The error histogram shows that most prediction errors are clustered around zero, indicating that the ANN effectively captured the relationship between inputs and outputs. The narrow and symmetrical distribution across training, validation, and testing sets reflects strong generalization and low overfitting risk. Although a few outliers exist, their impact is minimal, confirming the model's robustness and accuracy in predicting the thermal performance of the solar air collector.

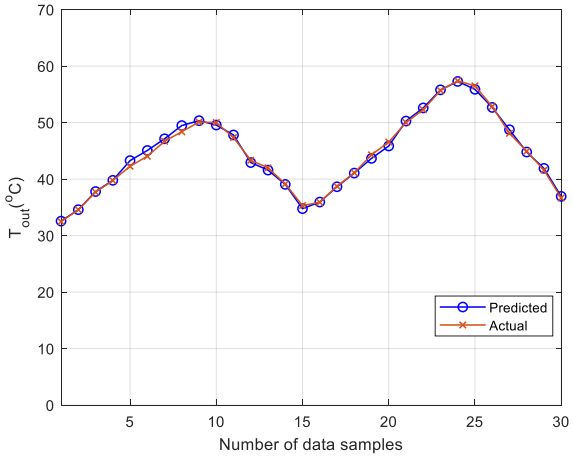
To further assess model performance, Figures 7 and 8 presents the comparison of actual and predicted values of outlet air temperature and efficiency, respectively. For each surface type, a total of 30 experimental data samples were used, corresponding to 15 measurements at a mass flow rate of 0.05 kg/s and 15 measurements at a mass flow rate of 0.025 kg/s. In these figures, the x-axis represents the number of data samples, while the y-axis corresponds to the experimental and ANN-predicted values of the respective parameters.



(**a**)

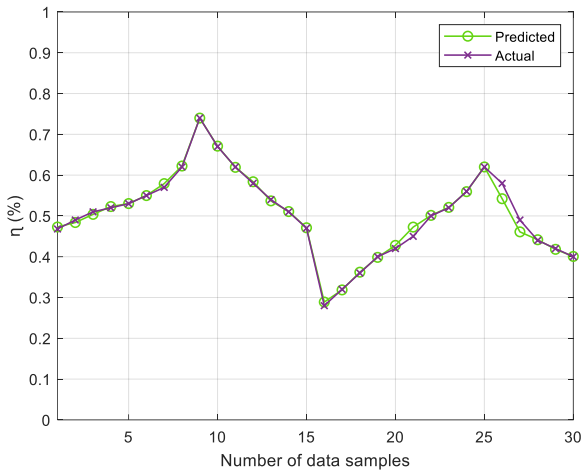


(**b**)

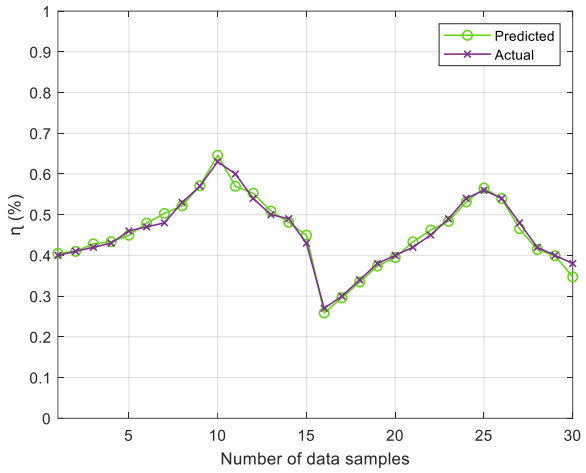


(**c**)

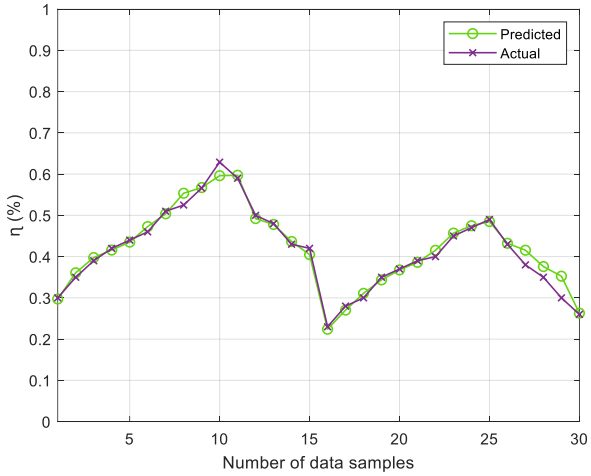
Figure 7. Comparison of outlet temperature of experimental and predicted data versus number of data samples. (**a**). Type I, (**b**). Type II, (**c**). Type III.



(**a**)



(**b**)



(**c**)

Figure 8. Comparison of efficiency of experimental and predicted data versus number of data samples. (**a**). Type I, (**b**). Type II, (**c**). Type III.

In Figure 7, the first 15 data samples correspond to the mass flow rate of 0.05 kg/s, while the remaining 15 samples correspond to 0.025 kg/s. Since the experiments were conducted between 9:00 a.m. and 4:00 p.m. at half-hour intervals, the outlet temperature

profile clearly follows the diurnal variation in solar irradiance. At the beginning of the tests in the morning, solar radiation was relatively low, which resulted in lower outlet temperatures. As the sun approached noon, the irradiance reached its maximum, leading to peak outlet temperatures. Toward the late afternoon, the solar radiation decreased and, consequently, the outlet temperature gradually dropped. This characteristic rise–fall trend is observed for both mass flow rates, although the absolute outlet temperatures differ depending on the airflow rate.

In contrast to the outlet air temperature trend shown in Figure 7, the thermal efficiency curve in Figure 8 exhibits a slightly different pattern. This is because efficiency is not solely a function of the outlet temperature, but also depends on the inlet temperature, solar irradiance, and mass flow rate. For example, higher solar irradiance increases the useful energy gain, but at the same time, a higher mass flow rate leads to a larger denominator in the efficiency expression, which may moderate the overall efficiency values. Similarly, variations in the inlet air temperature directly affect the temperature rise across the collector and therefore impact the efficiency. As a result, the efficiency trend does not exactly follow the outlet temperature variation but instead reflects the combined influence of all these operating parameters.

The data points align closely with the ideal diagonal line representing perfect agreement. This close alignment indicates that the model is capable of accurately replicating the actual system behavior across a range of operating conditions. The consistency observed in both parameters reinforces the reliability and precision of the ANN in modeling the thermal performance of the solar air collector equipped with porous absorber surfaces. Such strong correlation further suggests that the network has successfully learned the underlying relationships within the dataset.

Figure 9 shows the developed Simulink block diagram of the ANN prediction model. This model is utilized to generate the predicted values as listed in Table 1, together with the actual values. The values in row 8 are same as the Simulink model given in Figure 9.

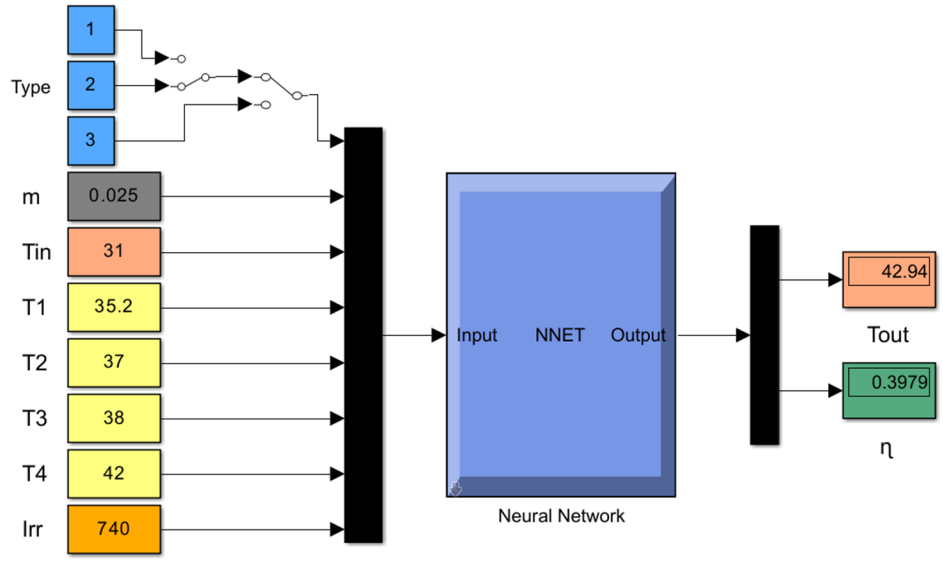


Figure 9. Simulink block diagram of the ANN prediction model with illustrative input–output values.

Table 1. Comparison between experimental and ANN-predicted values for selected test cases.

Sample	Inputs								Outputs			
									Tout		Efficiency	
	Surface Type	m (kg/s)	Tin (°C)	T + 1 (°C)	T2 (°C)	T3 (°C)	T4 (°C)	Irr (W/m^2)	Predicted (°C)	Actual (°C)	Predicted (%)	Actual (%)
1	1	0.05	35	36	36.5	37	38.2	480	39.56	39.29	0.46	0.46
2	1	0.025	40	42	46	51.5	56	933	58.93	58.57	0.52	0.52
3	1	0.05	30	37	39	40.9	41	850	42.48	42.70	0.54	0.54
4	1	0.025	33	37	39.4	41	42	833	46.70	47.19	0.42	0.44
5	1	0.05	36	41	43.2	45	49	952	50.20	50.00	0.63	0.62
6	1	0.025	28	32	33.5	34	38	700	38.79	38.81	0.38	0.40
7	2	0.05	35	37	38.5	40	41	765	41.95	41.76	0.49	0.46
8	2	0.025	34	39	42	45	46	830	48.19	47.54	0.44	0.42
9	2	0.05	30	31	32	33.2	34.3	680	35.03	35.70	0.40	0.43
10	2	0.025	31	35.2	37	38	42	740	42.94	42.42	0.39	0.40
11	2	0.05	42	43	45.9	47	49	900	51.98	51.82	0.57	0.57
12	2	0.025	40	45	48	53	56	890	58.26	58.62	0.52	0.54
13	3	0.05	35	36	39.4	41	42	862	42.85	43.33	0.50	0.50
14	3	0.025	38	42.5	44	47	50.1	905	53.02	52.28	0.41	0.40
15	3	0.05	30	30.9	31.3	31.6	32	432	33.07	32.47	0.37	0.30
16	3	0.025	32	33	34	34.5	35.2	440	36.71	35.89	0.27	0.23
17	3	0.05	40	42	45	48	49	937	49.31	50.11	0.57	0.56
18	3	0.025	37	39	41	44.3	48	861	50.16	50.00	0.38	0.39

Specifically, the numerical values shown in the figure (e.g., mass flow rate, inlet and surface temperatures, and irradiance) are taken from Table 1 and correspond to a particular operating condition. These values are presented as an illustrative example to demonstrate how the ANN processes the input parameters to predict the outlet air temperature and the thermal efficiency. To assess the effectiveness of the ANN model, the predicted output estimates were evaluated against the corresponding experimental findings under identical input conditions.

This comparison is systematically presented in Table 1, where both predicted and measured values are documented for a range of test cases. The close agreement between these values indicates the model's high predictive accuracy and its ability to effectively replicate the experimental outcomes.

Subsequently, the ANN model was re-assessed using the experimental dataset. High degree of agreement was found between the predicted outputs and the actual measurements, yielding a R of 0.99987 and a MSE of 0.0901, both of which indicate excellent predictive performance.

In Figure 10, the x-axis ("Target") represents the experimentally measured values, while the y-axis ("Output") corresponds to the values predicted by the ANN model. The dashed line (Y = T) indicates the ideal reference where predictions perfectly match the targets. This plot was obtained using 12 test data samples, which were randomly selected from the experimental dataset. The plot clearly demonstrates the alignment between experimental and predicted values during the testing phase.

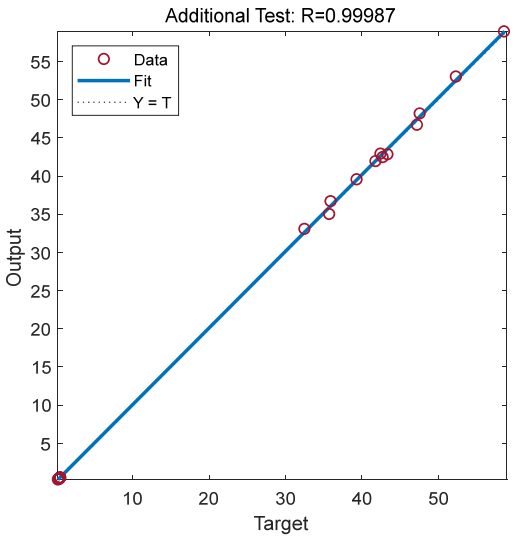


Figure 10. The correlation plot of the ANN model for the test dataset.

These simulation results demonstrate that the ANN model is highly effective in modeling the thermal performance of the solar air collector. The high R-values and low prediction errors validate the robustness and precision of the network. This model can be extended for optimization studies, parametric analyses, or real-time control systems in future work.

5. Conclusions

This study successfully developed and validated an ANN model to predict the outlet air temperature and thermal efficiency of a solar air collector equipped with porous metallic scourer absorber surfaces. The model was trained and tested using an extensive experimental dataset comprising three different absorber surface configurations and two distinct mass flow rates. The ANN demonstrated exceptional predictive performance, reflected by a high correlation coefficient (R = 0.99987) and a low mean squared error (MSE = 0.0901), confirming its ability to accurately replicate the complex thermal behavior of the system under various operating conditions.

By integrating multiple input variables (such as mass flow rate, inlet air temperature, solar irradiance, and surface temperatures measured at four points), the ANN effectively captured the nonlinear and multivariable relationships influencing the collector's performance. The strong correlation between predicted and experimental outputs, supported by both statistical metrics and graphical analysis, indicates the model's robustness, precision, and generalization capability without signs of overfitting or underfitting.

This research highlights the potential of ANN-based approaches as a fast, reliable, and cost-effective alternative to traditional modeling techniques and experimental trials for solar air collectors. In particular, it provides valuable insights into the performance forecasting and optimization of solar air collectors employing non-traditional porous absorber geometries, which enhance heat transfer through increased surface area and turbulence. Future work may focus on extending this ANN model for real-time control, optimization studies, and parametric analyses to further improve the configuration and efficiency of SAC systems.

However, the current study has certain limitations. The experiments were conducted under controlled conditions with limited ranges of solar irradiance and mass flow rates. Moreover, factors such as deformation of the collector materials, dust accumulation on the glass cover, shading effects, and variable weather fluctuations (e.g., strong wind or cloudy periods) were not considered in the present model but may reduce efficiency in

real-world applications. Therefore, further validation with expanded datasets covering different climatic zones, wider operating ranges, and long-term operation will be required to confirm the applicability of the model under diverse conditions.

Author Contributions: Conceptualization, F.O.; methodology, F.O. and A.D.; Software, Z.B.D. and H.G.; Validation, Z.B.D. and H.G.; Formal analysis, Z.B.D. and H.G.; Investigation, F.O. and A.D.; Data curation, F.O. and A.D.; Writing—original draft, F.O. and Z.B.D.; Writing—review & editing, Z.B.D. and H.G.; Visualization, Z.B.D. and H.G.; Supervision, H.G.; Project administration, Z.B.D.; Funding acquisition, Z.B.D. All authors have read and agreed to the published version of the manuscript.

Funding: This study was financially supported by the Scientific Research Projects Coordination Unit of Firat University (FÜBAP) under project number TEKF.24.55.

Data Availability Statement: The original contributions presented in the study are included in the article; further inquiries can be directed to the corresponding author.

Conflicts of Interest: The authors declare no conflicts of interest.

Abbreviations

The following abbreviations are used in this manuscript:

ANN	Artificial neural network
Irr	Solar irradiance
m	Mass flow rate
MSE	Mean squared error
PVT	Photovoltaic–thermal
R	Correlation coefficient
SAC	Solar air collectors
T_{in}	Inlet air temperature
T_{out}	Outlet air temperature
T_1, T_2, T_3, T_4	Different surface temperature
y_i , y_i'	Observed and predicted values
$\overline{y_i}$, $\overline{y_i'}$	Mean values of the observed and predicted data
η	Thermal efficiency

References

1. Kumar, P.G.; Vigneswaran, V.S.; Balaji, K.; Vinothkumar, S.; Prabakaran, R.; Sakthivadivel, D.; Kim, S.C. Augmented v-corrugated absorber plate using shot-blasting for solar air heater–Energy, Exergy, Economic, and Environmental (4E) analysis. *Process Saf. Environ. Prot.* **2022**, *165*, 514–531. [CrossRef]
2. Diao, Y.; Qi, N.; Wang, Z.; Zhao, Y.; Chen, C.; Wang, Z. Thermal performance analysis of a solar air collection–cascade storage system integrated with micro-heat pipe arrays. *Sol. Energy* **2021**, *224*, 1271–1290. [CrossRef]
3. Khanlari, A.; Güler, H.Ö.; Tuncer, A.D.; Şirin, C.; Bilge, Y.C.; Yılmaz, Y.; Güngör, A. Experimental and numerical study of the effect of integrating plus-shaped perforated baffles to solar air collector in drying application. *Renew. Energy* **2020**, *145*, 1677–1692. [CrossRef]
4. Khanlari, A.; Sözen, A.; Afshari, F.; Şirin, C.; Tuncer, A.D.; Gungor, A. Drying municipal sewage sludge with v-groove triple-pass and quadruple-pass solar air heaters along with testing of a solar absorber drying chamber. *Sci. Total Environ.* **2020**, *709*, 136198. [CrossRef] [PubMed]
5. Yadav, A.S.; Gattani, A. Solar thermal air heater for sustainable development. *Mater. Today Proc.* **2022**, *60*, 80–86. [CrossRef]
6. Yadav, A.S.; Agrawal, A.; Sharma, A.; Sharma, S.; Maithani, R.; Kumar, A. Augmented artificially roughened solar air heaters. *Mater. Today Proc.* **2022**, *63*, 226–239. [CrossRef]
7. Darici, S.; Kilic, A. Comparative study on the performances of solar air collectors with trapezoidal corrugated and flat absorber plates. *Heat Mass Transf.* **2020**, *56*, 1833–1843. [CrossRef]
8. Esen, H. Experimental energy and exergy analysis of a double-flow solar air heater having different obstacles on absorber plates. *Build. Environ.* **2008**, *43*, 1046–1054. [CrossRef]

9. Ghritlahre, H.K.; Chandrakar, P.; Ahmad, A. A comprehensive review on performance prediction of solar air heaters using artificial neural network. *Ann. Data Sci.* **2021**, *8*, 405–449. [CrossRef]
10. Luan, N.T.; Phu, N.M. Thermohydraulic correlations and exergy analysis of a solar air heater duct with inclined baffles. *Case Stud. Therm. Eng.* **2020**, *21*, 100672. [CrossRef]
11. Esen, H.; Ozgen, F.; Esen, M.; Sengur, A. Artificial neural network and wavelet neural network approaches for modelling of a solar air heater. *Expert Syst. Appl.* **2009**, *36*, 11240–11248. [CrossRef]
12. Diez, F.J.; Navas-Gracia, L.M.; Martínez-Rodríguez, A.; Correa-Guimaraes, A.; Chico-Santamarta, L. Modelling of a flat-plate solar collector using artificial neural networks for different working fluid (water) flow rates. *Sol. Energy* **2019**, *188*, 1320–1331. [CrossRef]
13. Delfani, S.; Esmaeili, M.; Karami, M. Application of artificial neural network for performance prediction of a nanofluid-based direct absorption solar collector. *Sustain. Energy Technol. Assess.* **2019**, *36*, 100559. [CrossRef]
14. Wang, W.; Li, M.; Hassanien, R.H.E.; Ji, M.E.; Feng, Z. Optimization of thermal performance of the parabolic trough solar collector systems based on GA-BP neural network model. *Int. J. Green Energy* **2017**, *14*, 819–830. [CrossRef]
15. Ghritlahre, H.K.; Prasad, R.K. Application of ANN technique to predict the performance of solar collector systems—A review. *Renew. Sustain. Energy Rev.* **2018**, *84*, 75–88. [CrossRef]
16. Castilla, M.; Redondo, J.L.; Martínez, A.; Álvarez, J.D. Artificial Neural Network-based digital twin for a flat plate solar collector field. *Eng. Appl. Artif. Intell.* **2024**, *133*, 108387. [CrossRef]
17. Sun, C.; Fares, M.N.; Sajadi, S.M.; Li, Z.; Jasim, D.J.; Hammoodi, K.A.; Alizadeh, A.A. Numerical examination of exergy performance of a hybrid solar system equipped with a sheet-and-sinusoidal tube collector: Developing a predictive function using artificial neural network. *Case Stud. Therm. Eng.* **2024**, *53*, 103828. [CrossRef]
18. Du, B.; Lund, P.D.; Wang, J. Improving the accuracy of predicting the performance of solar collectors through clustering analysis with artificial neural network models. *Energy Rep.* **2022**, *8*, 3970–3981. [CrossRef]
19. Naveenkumar, R.; Venkateshkumar, R.; Mohanavel, V.; Franklin, C.; Ismail, S.O.; Ravichandran, M.; Soudagar, M.E.M. Recent developments in solar water heaters and solar collectors: A review on experimental and neural network analysis. *Results Eng.* **2025**, *25*, 104394. [CrossRef]
20. Dayan, A. Energy and Exergy Analysis of an Air Solar Collector with Absorber Plate Made of Porous Material. Master's Thesis, Firat University, Elazig, Türkiye, 2021.
21. Duranay, Z.B.; Guldemir, H. Power Prediction in Photovoltaic Systems with Neural Networks: A Multi-Parameter Approach. *Appl. Sci.* **2025**, *15*, 3615. [CrossRef]
22. Aslan Topçuoglu, Y. Prediction of the effect of fly ash on the unconfined compressive strength of basalt fiber reinforced clay using artificial neural networks. *Processes* **2025**, *13*, 157. [CrossRef]
23. Sengur, D. Pedagogical othering and suicide: A preventive model proposal with machine learning approaches. *Int. Online J. Educ. Sci.* **2023**, *15*, 414–427.
24. Guldemir, N.H.; Alkan, A. Classification of optical coherence tomography images via deep learning. *Firat Univ. J. Eng. Sci.* **2021**, *33*, 607–615.
25. Ghritlahre, H.K.; Prasad, R.K. Prediction of heat transfer of two different types of roughened solar air heater using artificial neural network technique. *Therm. Sci. Eng. Prog.* **2018**, *8*, 145–153. [CrossRef]

Disclaimer/Publisher's Note: The statements, opinions and data contained in all publications are solely those of the individual author(s) and contributor(s) and not of MDPI and/or the editor(s). MDPI and/or the editor(s) disclaim responsibility for any injury to people or property resulting from any ideas, methods, instructions or products referred to in the content.